



HAL
open science

Two-dimensional metal structures revealed by evolutionary computations: Pb/Al 13 Co 4 (100) as a case study

Florian Brix, Émilie Gaudry

► To cite this version:

Florian Brix, Émilie Gaudry. Two-dimensional metal structures revealed by evolutionary computations: Pb/Al 13 Co 4 (100) as a case study. *Journal of Vacuum Science & Technology A*, 2022, 40 (1), pp.012203. 10.1116/6.0001439 . hal-03542016

HAL Id: hal-03542016

<https://hal.science/hal-03542016>

Submitted on 25 Jan 2022

HAL is a multi-disciplinary open access archive for the deposit and dissemination of scientific research documents, whether they are published or not. The documents may come from teaching and research institutions in France or abroad, or from public or private research centers.

L'archive ouverte pluridisciplinaire **HAL**, est destinée au dépôt et à la diffusion de documents scientifiques de niveau recherche, publiés ou non, émanant des établissements d'enseignement et de recherche français ou étrangers, des laboratoires publics ou privés.

Two-dimensional metal structures revealed by evolutionary computations: Pb/Al₁₃Co₄(100)s a case study

F. Brix¹ and E. Gaudry*¹

Université de Lorraine, CNRS, Institut Jean Lamour, Campus Artem, 2 allée André Guinier, 54000 Nancy, France

(*Electronic mail: Emilie.Gaudry@univ-lorraine.fr)

(Dated: 25 November 2021)

We have combined extensive Density Functional Theory calculations with an evolutionary algorithm to investigate possible structural models for two-dimensional (2D) Pb films supported on the Al₁₃Co₄(100) quasicrystal approximant surface. The minimization of the total energy with the constraint of maximizing the atomic density in the layer leads to 2D atomic arrangement with pentagonal motifs, reflecting the symmetry of the substrate. Our findings show that the 2D structure can be interpreted as a stable structure, with 16 Pb atoms per surface cell in the film, in accordance with the measured coverage. This conclusion is also supported by the reasonable agreement between the experimental STM images and those simulated using this structural model. Alternatively, a metastable 2D film made of 15 Pb atoms fits with the experimental observations. This study opens a route towards the prediction of supported complex 2D films.

This paper is dedicated to the memory of Pat Thiel, who has been a guide for so many of us

I. INTRODUCTION

Two-dimensional (2D) metallic films have attracted the interest of scientists from a large diversity of fields, due to their fascinating physical and chemical properties, owing to their high aspect ratio, their unique structures and possible quantum-size effects.^{1,2} They have potential applications in many domains such as catalysis, electronics/optoelectronic devices, sensing, and energy storage.

The close-packed structure of elemental metals, originating from the non-directional metallic bonding, is expected to be hardly compatible with 2D materials. However, many theoretical works predicted the existence of stable free-standing single-layer 2D metals (see^{3,4} and references therein). This is the case with lead, for which a buckled honeycomb structure with a potential topological character has been foreseen by Density Functional Theory (DFT).⁵⁻⁷ Nevertheless, the experimental growth of two-dimensional metal layers is not straightforward, and 2D metallic films are generally synthesized over a substrate.⁸ The latter is known to impact the atomic arrangements in 2D metal films. Focusing on ultrathin Pb films, several phases of Pb/Si(111) have been formed at room temperature with varying degrees of coverage up to 2 monolayers.⁹ On Al(111), the large mobility of Pb adatoms and the weak interaction with the substrate leads to the formation of a $(\sqrt{31} \times \sqrt{31})R8.95^\circ$ high-order commensurate structure (HOC structure).¹⁰ Less trivial 2D arrangements of Pb atoms are found on intermetallic substrates, such as the graphene-like structure obtained recently by Yuhara et al. on Pd_(1-x)Pb_x(111).¹¹ On quasicrystals, τ inflated quasiperiodic structures are generally observed.^{10,12}

Heterogeneous nucleation is a key factor that controls the epitaxial growth, through substrate-adsorbate interactions. Adsorbate-adsorbate and steric interactions, related to the size

of the adsorbates and how they can be accommodated by the substrate, are also identified to be crucial. While these general principles are well known, the prediction of epitaxial structures is still challenging. Considerable progress have been made in crystal structure prediction these last years, through the development of efficient computer codes and the availability of large computational resources. Methods such as annealing,^{13,14} evolutionary,^{15,16} swarm or basin/minima hopping^{14,17,18} based algorithms are able to escape the local minima to efficiently investigate the configuration space. These methods are increasingly used for bulk structures, but they are rarely employed for two-dimensional materials.^{19,20} Though, they can bring useful insights to analyze the experimental observations, as explained in this article.

In this work, we performed evolutionary computations to model 2D lead films supported on the Al₁₃Co₄(100) quasicrystalline approximant surface. We selected this intermetallic substrate, motivated by previous experimental and theoretical studies.^{21,22} When Pb deposition is achieved at 573 K, the ultrathin films are found to be quite well ordered, described by a periodic arrangement of irregular pentagons, in which the adsorbate-substrate interactions are conjectured to play a dominant role.²¹ The connected bipentagonal motifs, observed by scanning tunnelling microscopy (STM), are understood as being related to Al atomic arrangements on the clean surface. However, while the termination plane of the substrate contains four Al pentagonal motifs per surface cell, only two (larger) pentagonal features are visible in the experimental images. In addition, the STM images simulated from the structural model proposed so far, did not lead to satisfactory agreement with the experimental data.²² In this article, we show that the combination of Density Functional Theory (DFT) with evolutionary computations lead to stable two-dimensional Pb layers with pentagonal atomic arrangements, reflecting the symmetry of the substrate. The Pb atoms are not systematically located in most stable adsorption sites identified for atomic lead, but the structure of the Pb film results from the minimization of the total energy with the constraint of maximizing the atomic density in the film. Two structural

models lead to simulated STM images in good agreement with the experimental ones: a stable film made of 16 Pb atoms per surface cell and a metastable 2D layer containing 15 Pb atoms per surface cell.

II. MATERIALS AND METHODS

A. Structural model of Al₁₃Co₄ (100)

The Al₁₃Co₄ orthorhombic structure (*Pmn*2₁ space group) is described as a pile of two types of planes, perpendicular to the [100] direction, labeled alternatively flat-type (F-type) and puckered-type (P-type) planes.²³ The stacking sequence is F₀P_{0.25}F_{0.5}P_{0.75} and the interlayer distance is approximately 2 Å. On the other hand, the structure can be understood as a stacking of Henley-type clusters.^{24,25}

Several complementary techniques have been employed to provide a reliable model of the Al₁₃Co₄(100) surface. The combination of STM, Low Energy Electron Diffraction (LEED) and DFT calculations converged towards a surface terminating at puckered layers where on average all Al atoms are present and protruding Co atoms are missing.²⁶ The combination of surface X-ray diffraction and DFT pointed towards the same surface model, with partial occupancies for surface Co sites slightly buried in the P-type plane.²⁷

Specific atomic arrangements are found in the termination plane of Al₁₃Co₄(100). Aluminum atoms form pentagonal motifs (displayed with gray lines in Fig.2), connected 2 to 2 by squared patterns and thus leading to two Al bipentagonal motifs (BMs) per surface cell. The two Al BMs are not equivalent: one is located slightly below the mean position of the termination plane (BM-empty, shown in light gray, Fig. 2), while the second one, decorated with Co atoms buried in the pentagonal Al hollow sites, lies slightly above the mean position of the termination plane (BM-Co, shown in dark gray, Fig. 2).

B. Genetic algorithm

Our methodology is based on the evolutionary algorithm USPEX,^{28–30} which has already been used to predict the crystal structure of two-dimensional materials.^{19,20} Each structure was built with a 7-layer thick slab for the substrate (139 Al and 36 Co atoms in total, including 26 Al and 2 Co atoms in the termination plane), covered by a Pb film – thin region (2 Å thick) above the substrate – and a 11 Å void thickness. Several coverages have been considered : 14, 15, 16 and 17 Pb atoms per 1×1 surface cell. The positions of the atoms in the film were optimized, along with those in the topmost layer of the substrate. The initial structures of the film were generated randomly, and then built from variation operators that use the previous generation's best structures as parents, using operators such as Heredity (30%), Transmutation (10%) and Softmutation (10%). A few number of structures in a generation were produced randomly (50%) to diversify the population. All structures were relaxed by DFT (see below), using five

consecutive relaxation steps with increasing accuracy. Total energies were used to rank the final structures. An example is given in Fig.1 for the 15 Pb atom thin film structures. This process has been repeated cyclically until the best structures' set remains unchanged for 15 generations.

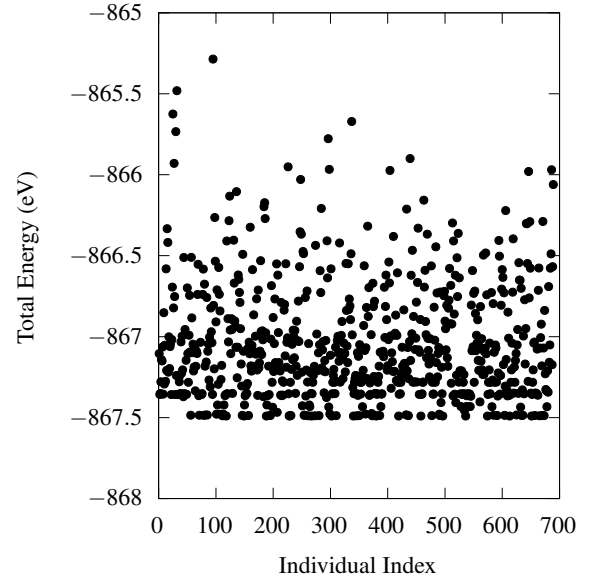


FIG. 1. Total energies of the 15 Pb atom thin film structures considered in this work.

C. Computational details

Total energy calculations were based on the Density Functional Theory (DFT) using the Vienna *ab initio* simulation package (VASP)^{31–33}. The interaction between the valence electrons and the ionic core was described using the spin polarized projector-augmented wave (PAW) method^{34,35} within the generalized gradient approximation of Perdew, Burke and Ernzerhof.³⁶ The valences of Pb, Al and Co were taken as 6s²6p², 3s²3p¹ and 3d⁸4s¹, respectively. In the final relaxation step, the one-electron Kohn-Sham orbitals were expanded with a kinetic energy cutoff of 450 eV. The reciprocal space integration was approximated with a Monkhorst-Pack k-point grid of 2×2×1. This computational setup lead to lattice parameters for bulk Al₁₃Co₄ in good agreement with the literature (*a*=8.195 Å, *b*=12.252Å, *c*=14.277Å).^{21,37}

D. Adsorption energies

In a first step, the adsorption of a single Pb atom has been computed on 400 specific points of a regular grid covering the Al₁₃Co₄(100) surface. For each point, the coordinates of the adsorbed Pb atom in the direction normal to the surface, as well as all degrees of freedom of the uppermost layer of the substrate have been allowed to relax during the geometry optimization process. The in-plane coordinates of the Pb

adsorbates have been frozen. For each point of the grid, the adsorption energy (E_{ads}^1) has been calculated by:

$$E_{ads}^1 = E_{Slab+Pb} - E_{Slab} - E_{SinglePb} \quad (1)$$

where $E_{Slab+Pb}$, E_{Slab} and $E_{SinglePb}$ are the total energies of the system {Slab+Pb}, of the clean slab and of a single Pb atom, respectively.

In a second step, the adsorption energies of Pb adlayers have been computed for several structures – single-layer thick Pb adlayer slab built by progressively filling all favorable adsorption sites,^{38,39} and models given by the structure prediction process – using the following equation:

$$E_{ads}^n = E_{slab+nPb} - E_{slab} - n \frac{E_{fccPb}}{4} \quad (2)$$

where n ($n > 1$) is the number of Pb atoms in the lead adlayer and E_{fccPb} is the cohesive energy of lead ($E_{fccPb} = -2.96$ eV). Our value for E_{fccPb} is in good agreement with other theoretical values calculated using the same methodology (-2.94 eV, -2.92 eV)^{39,40} and consistent with the experimental value (-2.03 eV).⁴¹

III. RESULTS

A. Surface energy landscape for a single Pb atom on Al₁₃Co₄(100)

The adsorption energy map, for a single Pb atom adsorbed on Al₁₃Co₄(100), is shown in Fig. 2.

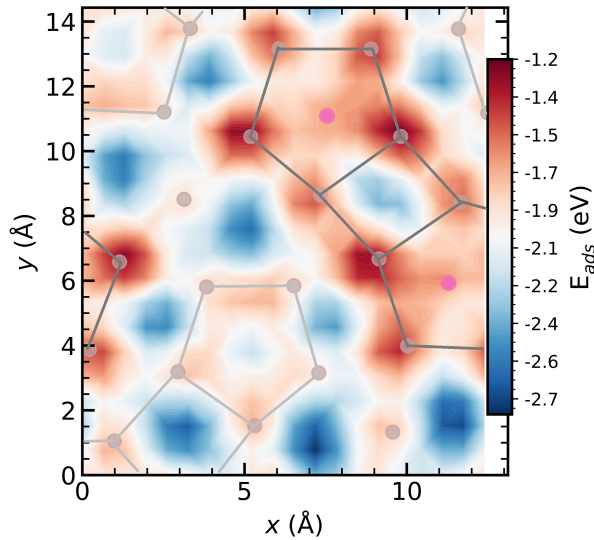


FIG. 2. Adsorption energy map for atomic Pb adsorbates on Al₁₃Co₄(100). Color code: Al = light gray, Co = pink. The BM-Co and BM-empty pentagonal motifs are shown in dark gray and light gray, respectively.

Overall, the interaction of atomic lead with the surface is favorable, all adsorption energies being negative, in the range

between -2.7 eV and -1.2 eV. The most favorable adsorption sites, with adsorption energies between -2.6 eV and -2.7 eV, are hollow sites. They are located outside the pentagonal aluminum arrangements (8 sites per surface unit cell) and in the center of squared arrangements of Al atoms (center of the BMs, 2 sites per surface unit cell). Sites located at the center of the Al pentagonal arrangement are found to be favorable as well, except when surface Co atoms are present. By the way, all sites located on top of a substrate's surface atoms are unfavorable. The worse case is found on top of Al atoms belonging to the BMs filled with Co atoms and located slightly above the mean position of the substrate's termination plane (BMs-Co): the corresponding adsorption energies lie in the range [-1.7;-1.2] eV. (Fig. 2). The top sites of the other BMs motifs, not containing any Co atom and located slightly below the mean position of the substrate's termination plane (BMs-empty), are less unfavorable, with adsorption energies close to -1.9 eV.

Thus, 12 favorable adsorption sites per surface unit cell are identified for atomic Pb. They are all located in hollow sites and thus are clearly driven by the topography of the substrate's termination plane. These results are consistent with the literature. Previous calculations indeed found the same most favorable adsorption sites, with similar adsorption energies (within 0.1 eV).²¹ These results are not specific to lead adsorption. Actually, a similar adsorption map plotted for atomic hydrogen on Al₁₃Co₄(100) identified distinct adsorption energies for hydrogen at the center of the Al pentagonal arrangements. However, no clear distinction between the two types of BMs has been noticed in this case.^{25,37}

B. Best structural models of supported Pb adlayers

At low coverage (less than 0.5 monolayer), the experimental results have been successfully interpreted by decorating the preferential adsorption sites.²¹ However, such an approach cannot explain the experimental observations at higher coverages, i.e. when the number of Pb atoms in the two-dimensional film is larger than the number of favorable adsorption sites.²² In the following, we show that in this case, evolutionary algorithms can provide realistic structural models.

The most stable Pb-adlayer structures containing 14, 15, 16 and 17 Pb atom per surface cell are gathered in Tab. I and Tab. II (appendix). Additional structures – metastable Pb-adlayers – are given in Tabs III-V (appendix). Our results show that the 1×1 surface cell can accommodate up to 16 Pb atoms. Indeed, the single layer character of the 2D Pb film is kept when $n \leq 16$ ($\Delta z \leq 2\text{\AA}$), and a second layer starts to grow when $n \geq 17$. The value of 16 Pb atoms per surface cell corresponds to the density of a fcc(111) plane. But the fcc arrangements of Pb atoms on Al₁₃Co₄(100) are not favored energetically, even if the average size mismatch between Pb(111) and Al₁₃Co₄(100) is small (the average value for the in-plane cell parameters is below 2.5%).

The superposition of the atomic adsorption map with the positions of the lead atoms in the 2D films shows that most

favorable atomic adsorption sites are filled by Pb atoms. Thus, in all 2D films, Pb arrangements form distorted pentagonal motifs, driven by the local symmetries of the Al₁₃Co₄(100) termination. Less stable sites are also occupied by Pb atoms in the 2D metal films, such as the sites on top of surface Co atoms, as well as bridge sites in the squared motif in between two Al pentagonal arrangements.

The adsorption energies per surface area (E_{ads}/A) are of the order of -30 meV/Å² for all structures with $n \leq 16$ (Fig. 3). It means that the interaction between the 2D Pb-layer and the substrate is much stronger with structurally optimized structures than with structures obtained by progressively filling all favorable adsorption sites, as performed in a previous study ($\simeq -13$ meV/Å²).³⁹ In addition, with increasing n , the interaction between the 2D-layer and the substrate becomes weaker and the Pb-Pb interaction gradually takes (more) control over the adlayer structure. For Pb atomic densities between 0.8 at/Å² and 0.9 at/Å² (14 to 16 at./surf. cell), the adsorption energy increases smoothly as a function of n . It suggests that part of most stable sites are filled first and that a compromise is then found to ensure a dense packing in the 2D Pb-layer while minimizing the total energy. For instance, the Pb atom located in the favorable hollow site labelled 'Init' (tab. I) in the 15 Pb atom film is shifted from its position in the 16 Pb atom film due to the presence of a close Pb atom (positions labelled 'Fin1' and 'Fin2'). The weakening of the adsorption is larger for $n=17$, consistently with the growth of a second Pb layer.

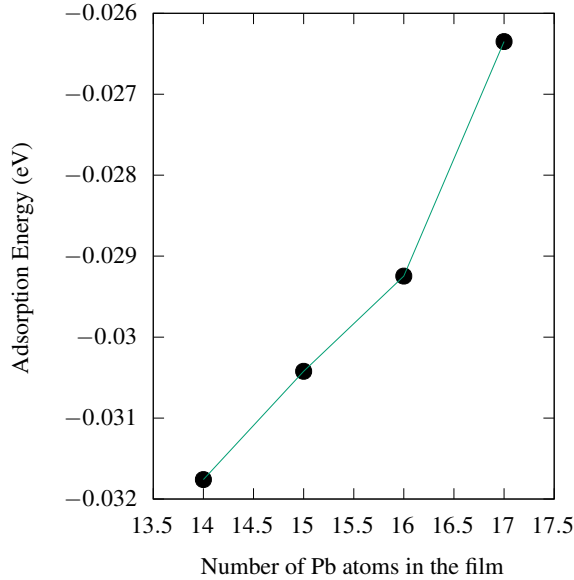


FIG. 3. Adsorption energies of the most stable Pb films.

The adhesion energy, i.e. the required energy (per unit area) to separate the slabs and create two free surfaces has been calculated for the stable 16 Pb atom layer using

$$E_{adh}(nPb) = E_{slab+nPb} - E_{slab} - E_{nPb} \quad (3)$$

with E_{nPb} the energy of the free-standing Pb film

($E_{slab+nPb}$ and E_{slab} are defined in Section II.D). We find $E_{adh}(16Pb)=1.33$ J/m². This value is much larger than the one calculated for the exfoliation of one graphene layer from graphite (0.425 J/m², 0.22 J/m², 0.23 J/m²)⁴²⁻⁴⁴. Thus, isolating a free-standing Pb layer with local 5fold symmetries, using a Pb layer grown on a quasicrystal approximant surface, seems unlikely.

C. Simulated STM images

The STM images have been simulated within the Tersoff-Hamman approximation ($V_{bias} = +1$ V),^{45,46} for a large number of structural models (Tabs. I-V). Overall, the simulated STM images are very diverse, the bright contrasts being very sensitive to the precise location of the Pb atoms (especially the height). Very few images show pentagonal features.

Distorted pentagonal bright features are visible in the STM image calculated from the most stable 16 Pb atom adlayer (dark gray motif shown in Tab. I). A better agreement with the experimental observations is observed for the STM image simulated from a metastable 15 Pb atom adlayer (Fig. 4). The averaged edge length of the pentagonal motifs is 4.02 Å, i.e. it is consistent with the value measured on the experimental image (4.83 Å).²¹ In both cases, the bright contrast of the pentagonal features is attributed to Pb atoms in the adsorption sites of the BM-Co motif, with the exception of the hollow site above the subsurface Co atom, which gives a dark contrast because of its lower height. Similarly, the favorable adsorption sites in the vicinity of the BM-empty motif, which are filled by Pb atoms, are not visible in the simulated STM images because they are positioned below the mean position of the plane.

The energy difference between the 15 Pb atom metastable structure and the 15 Pb atom most stable one is quite small ($\Delta E \simeq 9$ meV / Pb atom, Tab.IV). Such a small energy difference can be attributed to entropy. Vibrational contributions are known to have a stabilizing effect, whose magnitude is of the order of a few tens of percent of the surface energy – 10% at 973 K for the low-index surfaces of GaAs and InAs,⁴⁷ 30% at the melting point for the low-index surfaces of iron.¹⁸ A few percent (5%) of the surface energy of lead ($\gamma_{Pb(111)}$ 17.2 meV/Å²)^{48,49} is thus enough to account for ΔE here.

Finally, we should notice that the periodic boundary conditions enforced in the calculations may have possible effects in the STM images. The surface of the substrate is periodic, but this periodicity do not necessarily applies in the Pb film. This could explain some differences between the simulated and observed experimental STM images.

IV. CONCLUSION

In this work, evolutionary computations have been performed to offer a surface model for the 2D metal quasicrystal approximant grown on Al₁₃Co₄(100). The minimization of the total energy with the constraint of maximizing the atomic density in the layer leads to 2D atomic arrangement

with pentagonal motifs, reflecting the symmetry of the substrate. Adsorbate-adsorbate interactions play a non negligible role in the emergence of the ordered 2D metal structure, since several most favorable adsorption sites identified for the Pb atomic adsorption are not filled any more in the metal film, to optimize the film density. The pentagonal bright features in the experimental STM image are attributed to the Pb atoms located in the vicinity of the substrate BM-Co motif. Lead atoms adsorbed above the substrate BM-empty motif, appear with a dark contrast in the simulated STM image, because of their lower height.

Our study shows that it is possible to successfully predict the structure of 2D films with a rather good accuracy, based on extensive DFT calculations combined with evolutionary algorithms. This is very promising for the determination of more complex 2D films, such as 2D oxide films, made of two or more chemical elements.

ACKNOWLEDGMENTS

This work is supported by the European Integrated Center for the Development of New Metallic Alloys and Compounds. We acknowledge financial support through the COMETE project (CONception in silico de Matériaux pour l'Environnement et l'Énergie) co-funded by the European Union under the program FEDER-FSE Lorraine et Massif des Vosges 2014-2020. This work was granted access to the HPC resources of TGCC, CINES and IDRIS under the allocation 99642 attributed by GENCI (Grand Equipement National de Calcul Intensif). High Performance Computing resources were also partially provided by the EXPLOR centre hosted by the University de Lorraine (project 2017M4XXX0108).

DATA AVAILABILITY STATEMENT

The data that support the findings of this study are available from the corresponding author upon reasonable request.

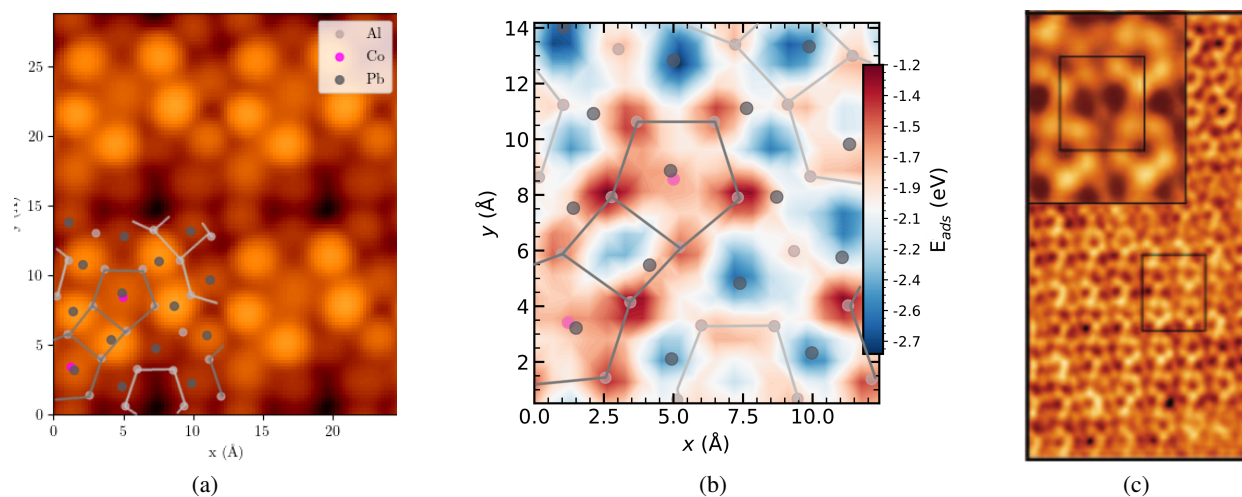


FIG. 4. (a) Simulated STM image of the metastable 15 Pb atom 2D film on Al₁₃Co₄(100) ($V_{bias}=+1$ V). (b) Corresponding structural model, superimposed with the atomic adsorption map. Color code: Pb = dark gray, Al = light gray, Co = pink. (c) High-resolution STM image of the 2D Pb layer at 573 K on Al₁₃Co₄(100): 18×9 nm² and 2.6×3.2 nm² (inset). Adapted from R. Addou, A. K. Shukla, S. Alarcón-Villaseca, É. Gaudry, T. Deniozou, M. Heggen, M. Feuerbacher, R. Widmer, O. Gröning, V. Fournée, J.-M. Dubois, and J. Ledieu, "Lead adsorption on the Al₁₃Co₄(100) surface: Heterogeneous nucleation and pseudomorphic growth," *New J. Phys.* 13, 103011 (2011). ©IOP Publishing and Deutsche Physikalische Gesellschaft. Reproduced by permission of IOP Publishing. All rights reserved.

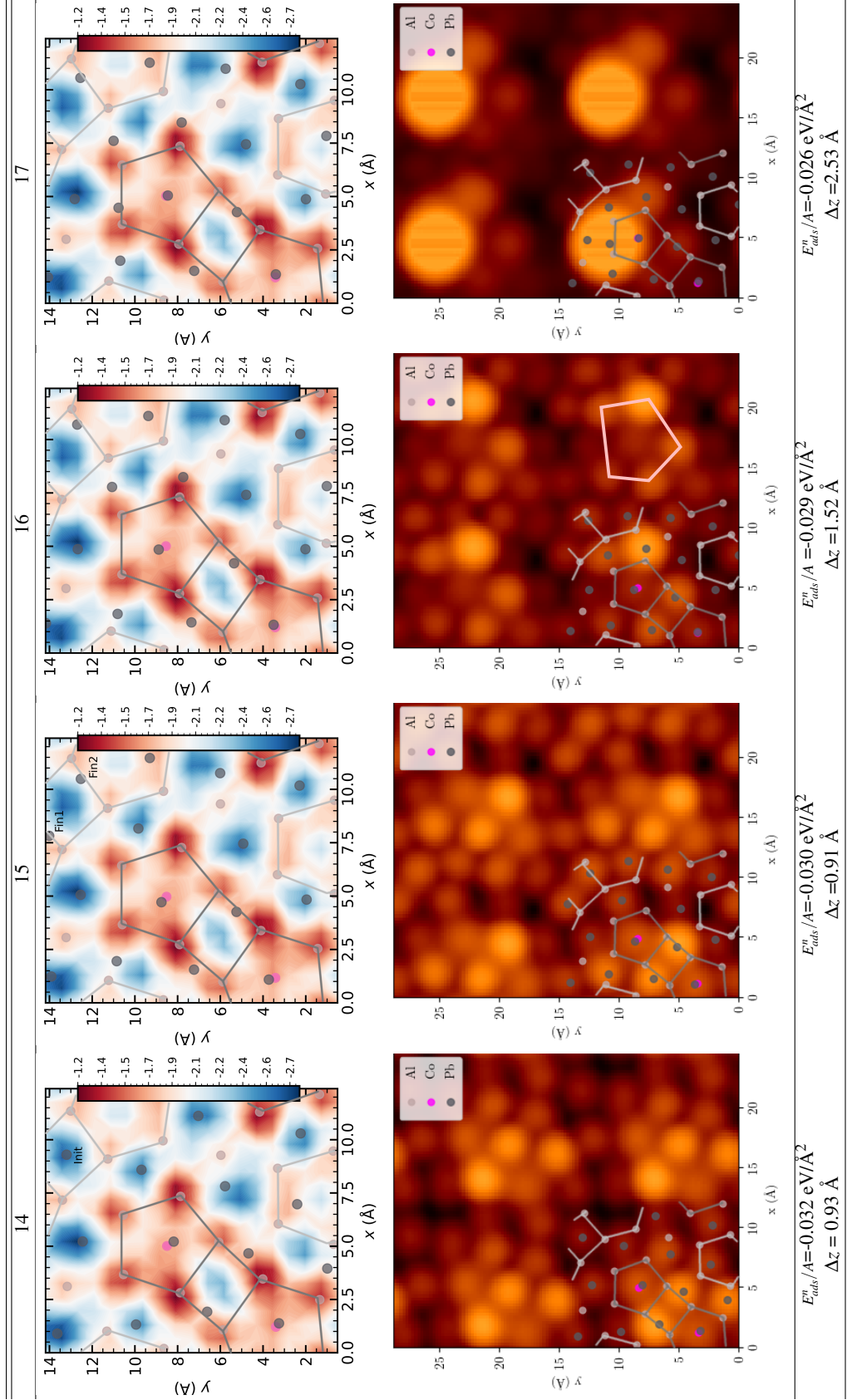


TABLE I. Best structural models calculated for 14, 15, 16 and 17 Pb atoms deposited on Al₁₃Co₄(100). The adsorption energies per surface area (E_{ads}^n/A) and the thicknesses of the Pb-adlayer (Δz) are given in each case, along with the simulated STM images. A pentagonal motif is shown in white (STM image of the 16-atom Pb adlayer). Color code: Pb = dark gray, Al = light gray, Co = pink. See text for the labels 'Init', 'Fin1' and 'Fin2'.

APPENDIX: BEST STRUCTURES FOR THE 2D PB FILM ON AL₁₃CO₄ (100)

n	top view	side view
14		
15		
15 (metastable)		
16		
17		

TABLE II. Best structures for the 2D Pb film on Al₁₃Co₄(100).

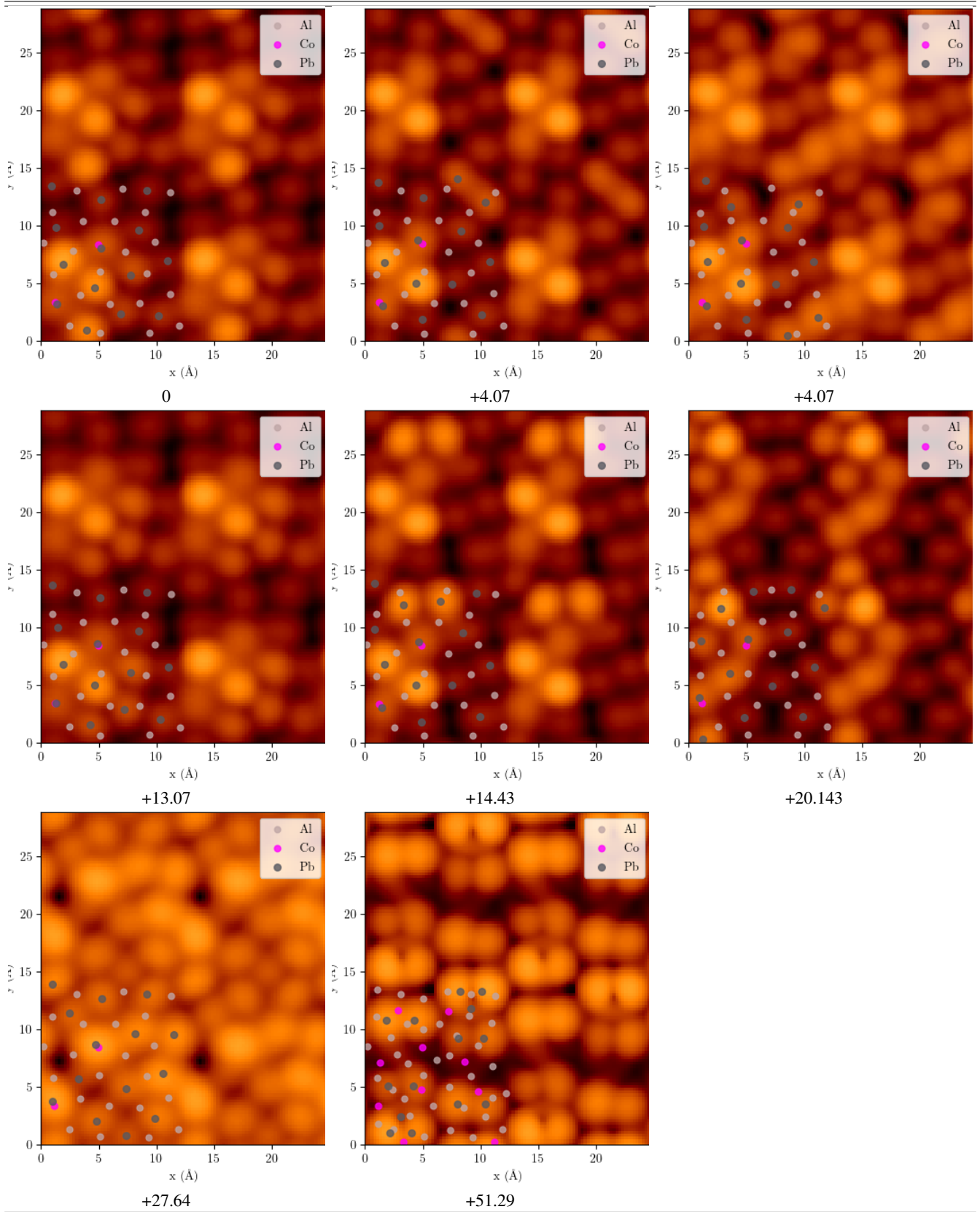


TABLE III: Several structures obtained in the last generation for a Pb-adlayer containing 14 atoms. Energy differences (in meV per Pb atom) are given in each case, relatively to the most stable structure.

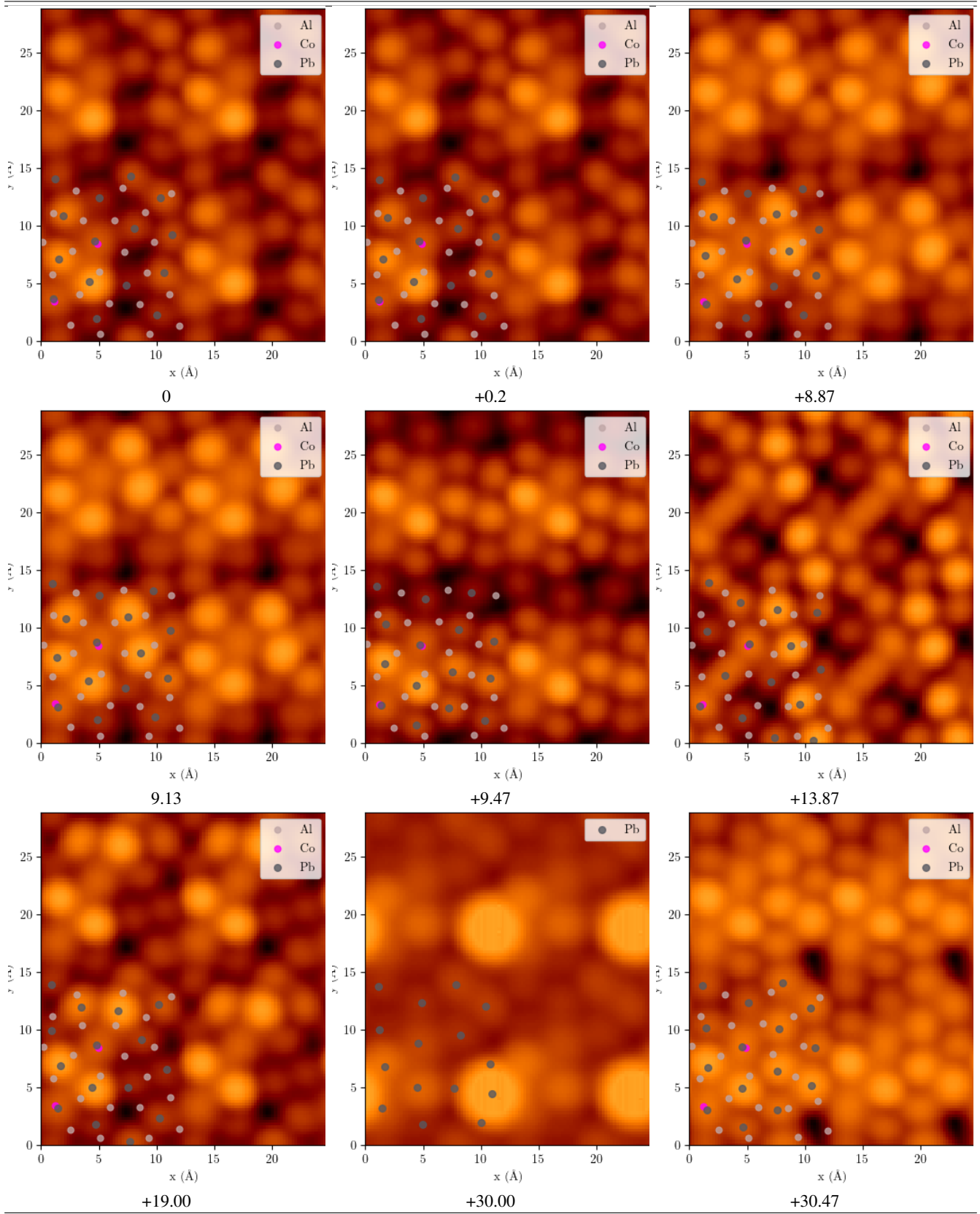


TABLE IV: Several structures obtained in the last generation for a Pb-adlayer containing 15 atoms. Energy differences (in meV per Pb atom) are given in each case, relatively to the most stable structure.

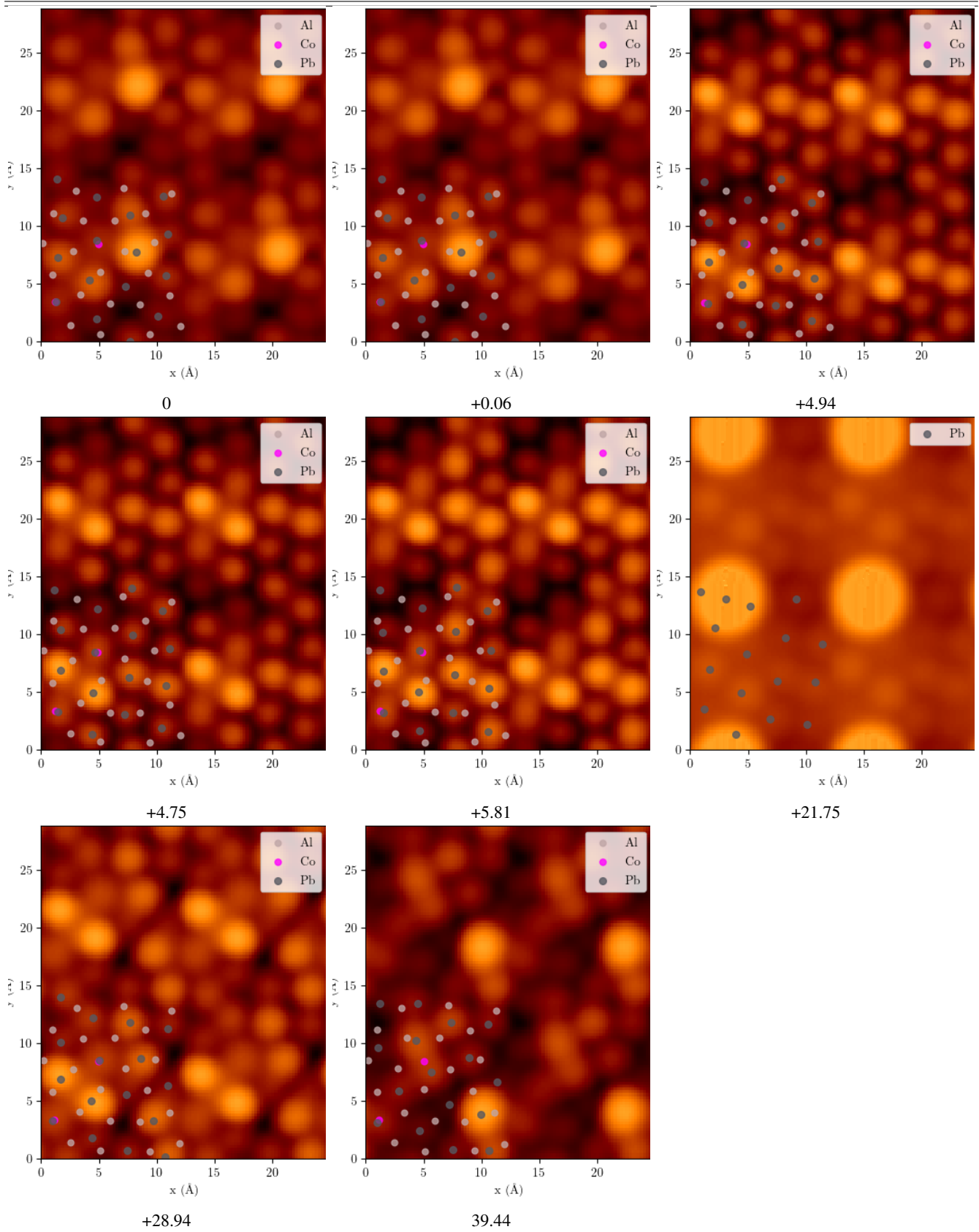


TABLE V: Several structures obtained in the last generation for a Pb-adlayer containing 16 atoms. Energy differences (in meV per Pb atom) are given in each case, relatively to the most stable structure.

- ¹Z. Fan, X. Huang, C. Tan, and H. Zhang, "Thin Metal Nanostructures: Synthesis, Properties and Applications," *Chem. Sci.* **6**, 95–111 (2015).
- ²T. Ling, J.-J. Wang, H. Zhang, S.-T. Song, Y.-Z. Zhou, J. Zhao, and X.-W. Du, "Freestanding Ultrathin Metallic Nanosheets: Materials, Synthesis, and Applications," *Adv. Mater.* **27**, 5396–5402 (2015).
- ³Q. Yu and Y. Yang, "Synthesis of Two-dimensional Metallic Nanosheets: From Elemental Metals to Chemically Complex Alloys," *ChemNanoMat* **6**, 1683–1711 (2020).
- ⁴F. Bechstedt, P. Gori, and O. Pulci, "Beyond graphene: Clean, hydrogenated and halogenated silicene, germanene, stanene, and plumbene," *Prog. Surf. Sci.* **96**, 1006615 (2021).
- ⁵P. Rivero, J.-A. Yan, V. M. García-Suárez, J. Ferrer, and S. Barraza-Lopez, "Stability and properties of high-buckled two-dimensional tin and lead," *Phys. Rev. B* **90**, 241408 (2014).
- ⁶X.-L. Yu, L. Huang, and J. Wu, "From a normal insulator to a topological insulator in plumbene," *Phys. Rev. B* **95**, 125113 (2017).
- ⁷Z.-Q. Huang, C.-H. Hsu, F.-C. Chuang, Y.-T. Liu, H. Lin, W.-S. Su, V. Ozolins, and A. Bansil, "Strain driven topological phase transitions in atomically thin films of group IV and V elements in the honeycomb structures," *New J. Phys.* **16**, 105018 (2014).
- ⁸T. Wang, M. Park, Q. Yu, J. Zhang, and Y. Yang, "Stability and synthesis of 2D metals and alloys: a review," *Mater. Today Adv.* **8**, 100092 (2020).
- ⁹W. B. Su, C. S. Chang, and T. T. Tsong, "Quantum size effect on ultra-thin metallic films," *J. Phys. D: Appl. Phys.* **43**, 013001 (2009).
- ¹⁰T. Deniozou, J. Ledieu, V. Fournée, D. Wu, T. A. Lograsso, H. T. Li, and R. D. Diehl, "Aperiodic and modulated pb thin films on fivefold icosahedral Al-Cu-Fe and Al(111): Tailoring the structure of Pb," *Phys. Rev. B* **79**, 245405 (2009).
- ¹¹J. Yuhara, B. He, N. Matsunami, M. Nakatake, and G. LeLay, "Graphene Latest Cousin: Plumbene Epitaxial Growth on a Nano WaterCube," *Adv. Mater.* **31**, 1901017 (2019).
- ¹²R. McGrath, H. R. Sharma, J. A. Smerdon, and J. Ledieu, "The memory of surfaces: epitaxial growth on quasi-crystals," *Phil. Trans. R. Soc. A* **370**, 2930–2948 (2012).
- ¹³J. Schön and M. Jansen, "Possible Existence of Alkali Metal Orthocarbonates at High Pressure," *Z. Kristal.* **216**, 307 (2001).
- ¹⁴G. E. Santoro, R. Martonak, E. Tosatti, and R. Car, "Theory of quantum annealing of an ising spin glass," *Science* **295**, 2427 (2002).
- ¹⁵A. Oganov and C. Glass, "Crystal structure prediction using evolutionary algorithms: principles and applications," *J. Chem. Phys.* **124**, 244704 (2006).
- ¹⁶D. M. Deaven and K.-M. Ho, "Molecular Geometry Optimization with a Genetic Algorithm," *Phys. Rev. Lett.* **75**, 288 (1995).
- ¹⁷Y. Wang, J. Lv, L. Zhu, and Y. Ma, "CALYPSO: A method for crystal structure prediction," *Comput. Phys. Commun.* **183**, 2063 (2012).
- ¹⁸S. Schönecker, X. Li, B. Johansson, S.-K. Kwon, and L. Vitos, "Thermal surface free energy and stress of iron," *Sci. Rep.* **5**, 14860 (2015).
- ¹⁹X.-F. Zhou, A. R. Oganov, Z. Wang, I. A. Popov, A. I. Boldyrev, and H.-T. Wang, "Two-dimensional magnetic boron," *Phys. Rev. B* **93**, 085406 (2016).
- ²⁰A. B. Mazitov and A. R. Oganov, "Evolutionary algorithm for prediction of the atomic structure of two-dimensional materials on substrates," preprint arXiv:2103.07677 (2021).
- ²¹R. Addou, A. K. Shukla, S. Alarcón-Villaseca, É. Gaudry, T. Deniozou, M. Heggen, M. Feuerbacher, R. Widmer, O. Gröning, V. Fournée, J.-M. Dubois, and J. Ledieu, "Lead adsorption on the Al₁₃Co₄ (100) surface: Heterogeneous nucleation and pseudomorphic growth," *New J. Phys.* **13**, 103011 (2011).
- ²²S. Alarcón-Villaseca, J.-M. Dubois, and E. Gaudry, "Lead adsorption on the pseudo-tenfold surface of the Al₁₃Co₄ complex metallic alloy: A first principle study," *Int. J. Quantum Chem.* **113**, 840–846 (2013).
- ²³J. Grin, U. Burkhardt, M. Ellner, and K. Peters, "Crystal Structure of Orthorhombic Co₄Al₁₃," *J. Alloys Compd.* **206**, 243–247 (1994).
- ²⁴P. Scheid, C. Chatelier, J. Ledieu, V. Fournée, and E. Gaudry, "Bonding Network and Stability of Clusters: The Case Study of the Al₁₃TM₄ Pseudo-10fold Surfaces," *Acta Crystallogr. A* **75**, 314–324 (2019).
- ²⁵C. Chatelier, Y. Garreau, A. Vlad, J. Ledieu, A. Resta, V. Fournée, M.-C. de Weerd, A. Coati, and E. Gaudry, "The pseudo-twofold surface of the Al₁₃Co₄ catalyst: structure, stability, and hydrogen adsorption," *ACS Appl. Mater. Interfaces* **12**, 39787–39797 (2020).
- ²⁶H. Shin, K. Pussi, É. Gaudry, J. Ledieu, V. Fournée, S. Alarcón-Villaseca, J.-M. Dubois, Y. Grin, P. Gille, W. Moritz, and R. Diehl, "Structure of the Orthorhombic Al₁₃Co₄(100) Surface Using LEED, STM and Ab Initio Studies," *Phys. Rev. B* **84**, 085411 (1to11) (2011).
- ²⁷E. Gaudry, C. Chatelier, G. McGuirk, L. S. Loli, M.-C. DeWeerd, J. Ledieu, V. Fournée, R. Felici, J. Drnec, G. Beutier, and M. de Boissieu, "Structure of the Al₁₃Co₄(100) Surface: Combination of Surface X-Ray Diffraction and Ab Initio Calculations," *Phys. Rev. B* **94**, 165406 (2016).
- ²⁸C. W. Glass, A. R. Oganov, and N. Hansen, "Uspex—evolutionary crystal structure prediction," *Comput. Phys. Commun.* **175**, 713–720 (2006).
- ²⁹A. O. Lyakhov, A. R. Oganov, H. T. Stokes, and Q. Zhu, "New developments in evolutionary structure prediction algorithm uspx," *Comput. Phys. Commun.* **184**, 1172–1182 (2013).
- ³⁰A. R. Oganov, A. O. Lyakhov, and M. Valle, "How evolutionary crystal structure prediction works and why," *Acc. Chem. Res.* **44**, 227–237 (2011).
- ³¹G. Kresse and J. Hafner, "Ab initio molecular dynamics for liquid metals," *Phys. Rev. B* **47**, 558 (1993).
- ³²G. Kresse and J. Furthmüller, "Efficiency of ab-initio total energy calculations for metals and semiconductors using a plane-wave basis set," *Comput. Mater. Sci.* **6**, 15–50 (1996).
- ³³G. Kresse and J. Furthmüller, "Efficient iterative schemes for ab initio total-energy calculations using a plane-wave basis set," *Phys. Rev. B* **54**, 11169 (1996).
- ³⁴P. E. Blöchl, "Projector augmented-wave method," *Phys. Rev. B* **50**, 17953 (1994).
- ³⁵G. Kresse and D. Joubert, "From ultrasoft pseudopotentials to the projector augmented-wave method," *Phys. Rev. B* **59**, 1758–1775 (1999).
- ³⁶J. P. Perdew, K. Burke, and M. Ernzerhof, "Generalized gradient approximation made simple [phys. rev. lett. 77, 3865 (1996)]," *Phys. Rev. Lett.* **78**, 1396–1396 (1997).
- ³⁷D. Kandaskalov, V. Fournée, J. Ledieu, and E. Gaudry, "Catalytic semihydrogenation of acetylene on the (100) surface of the o-al13co4 quasicrystalline approximant: density functional theory study," *J. Phys. Chem.* **121**, 18738–18745 (2017).
- ³⁸S. A. Villaseca, J.-M. Dubois, and É. Gaudry, "Lead adsorption on the pseudo-10-fold surface of the al13co4 complex metallic alloy: A first principle study," *International Journal of Quantum Chemistry* **113**, 840–846 (2013).
- ³⁹K. Anand, V. Fournée, G. Prévot, J. Ledieu, and E. Gaudry, "Non-Wetting Behavior of Al-Co Quasicrystalline Approximants Owing to their Unique Electronic Structures," *Appl. Mater. Inter.* **12**, 15793–15801 (2020).
- ⁴⁰K. Lejaeghere, V. V. Speybroeck, G. V. Oost, and S. Cottenier, "Error estimates for solid-state density-functional theory predictions: an overview by means of the ground-state elemental crystals," *Crit. Rev. Solid State Mater. Sci.* **39**, 1–24 (2014).
- ⁴¹C. Kittel, *Introduction to Solid State Physics*, 7th ed. (John Wiley & Sons, USA, 1996).
- ⁴²Y. Han, K. Lai, A. Lii-Rosales, M. Tringides, J. Evans, and P. Thiel, "Surface energies, adhesion energies, and exfoliation energies relevant to copper-graphene and copper-graphite systems," *Surf. Sci.* **685**, 48–58 (2019).
- ⁴³J. Wang, D. S. S. Jeon, A. Belianinov, S. V. Kalinin, A. P. Baddorf, and P. Maksymovych, "Atomic intercalation to measure adhesion of graphene on graphite," *Nat Commun* **7**, 13263 (2016).
- ⁴⁴E. Koren, E. Lörtscher, C. Rawlings, A. W. Knoll, and U. Duerig, "Adhesion and friction in mesoscopic graphite contacts," *Science* **348**, 679–683 (2015).
- ⁴⁵J. Tersoff and D. R. Hamann, "Theory and Application for the Scanning Tunneling Microscope," *Phys. Rev. Lett.* **50**, 1998–2001 (1983).
- ⁴⁶J. Tersoff and D. R. Hamann, "Theory of the scanning tunneling microscope," *Phys. Rev. B* **31**, 805–813 (1985).
- ⁴⁷I. Yeu, G. Han, J. Park, C.-S. Hwang, and J. Choi, "Equilibrium crystal shape of GaAs and InAs considering surface vibration and new (111)B reconstruction: ab-initio thermodynamics," *Sci. Rep.* **9**, 1127 (2019).
- ⁴⁸D. Yu and M. Scheffler, "First-Principles Study of Low-Index Surfaces of Lead," *Phys. Rev. B* **70**, 155417 (1to9) (2004).
- ⁴⁹D. Yu and H. P. Bonzel and M. Scheffler, "Orientation-dependent surface and step energies of Pb from first principles," *Phys. Rev. B* **74**, 115408 (2006).
- ⁵⁰J. Ledieu and L. Leung and L. H. Wearing and R. McGrath and T. A. Lo-

- grasso and D. Wu and V. Fournée, “Self-assembly, structure, and electronic properties of a quasiperiodic lead monolayer,” *Phys. Rev. B* **77**, 073409 (2008).
- ⁵¹D. J. Wales and H. A. Scheraga, “Global optimization of clusters, crystals, and biomolecules,” *Science* **285**, 1368 (1999).
- ⁵²S. Goedecker, *J. Chem. Phys.* **120**, 9911 (2004).
- ⁵³R. Addou, A. Shukla, S. A. Villaseca, É. Gaudry, T. Deniozou, M. Heggen, M. Feuerbacher, R. Widmer, O. Gröning, V. Fournée, *et al.*, “Lead adsorption on the Al₁₃Co₄ (100) surface: heterogeneous nucleation and pseudomorphic growth,” *New J. Phys.* **13**, 103011 (2011).
- ⁵⁴W. Wang, S. Dai, X. Li, J. Yang, D. Srolovitz, and Q. Zheng, *Nat. Commun.* **6**, 7853 (2015).
- ⁵⁵F. Schulte, *Surf. Sci.* **55**, 427 (1976).